Available online at www.sciencedirect.com
ScienceDirect
International Journal of Multiphase Flow 34 (2008) 102–109
International Journal of Multiphase Flow
www.elsevier.com/locate/ijmulflow

Brief communication

Deformation of a compound drop through a contraction in a pressure-driven pipe flow

Chunfeng Zhou [a], Pengtao Yue [a,b], James J. Feng [a,b,*]

[a] Department of Chemical and Biological Engineering, University of British Columbia, Vancouver, BC, Canada V6T 1Z3
[b] Department of Mathematics, University of British Columbia, Vancouver, BC, Canada V6T 1Z2

Received 30 May 2007; received in revised form 19 September 2007

1. Introduction

A compound drop consists of an inner drop enclosed in a shell of an immiscible liquid. When a large number of compound drops are suspended in another liquid medium, the resulting mixture is known as a double or multiple emulsion. Water-in-oil-in-water (W/O/W) emulsions have received much attention since they were proposed as a drug delivery vehicle for insulin (Engel et al., 1968). Previous studies on W/O/W emulsions have been mostly concerned with formulation and stabilization (Jiao and Burgess, 2003; Onuki et al., 2004; Bozkir and Hayta, 2004), and relatively little has been done on the deformation and morphological evolution of compound drops in flow fields. The latter process is practically important since shear-induced burst of the oil shell is an important mechanism for drug release (Muguet et al., 2001). The hydrodynamics of the multiple interfaces is also central to the preparation of multiple emulsions, either through intense shearing in a mixer (Goubault et al., 2001) or through compound jet breakup in microfluidic devices (Utada et al., 2005; Zhou et al., 2006). Finally, compound drop dynamics is relevant to the deformation and migration of eukaryotic cells, with the inner drop representing the cell nucleus suspended in the cytoplasm (Kan et al., 1998; Khismatullin and Truskey, 2005; Jadhav et al., 2005).

For the most part, fluid mechanical studies of compound drops have dealt with three types of flow geometries: translation in a quiescent fluid (Johnson and Sadhal, 1985), dynamics in extensional flows (Stone and Leal, 1990; Kan et al., 1998), and dynamics in shear flows (Stroeve and Varanasi, 1984; Smith et al., 2004). In particular, Kan et al. (1998) investigated the deformation, relaxation and breakup in uniaxial elongation, and interpreted the coupling between the inner drop and the outer shell in terms of two time scales. If the relaxation time of the inner drop matches that of the shell, the compound drop will behave like a homogeneous one. Toose et al. (1999) incorporated non-Newtonian rheology into the shell fluid and computed the deformation of the compound drop in elongational flow. More recently, Smith et al. (2004) constructed a phase diagram depicting the morphology of daughter drops after shear-induced breakup at various values of the capillary number and interfacial tension ratio between the inner and outer surfaces. Notably, all prior work has been done in *homogeneous* far-field flows. Little is known about compound drop deformation caused by *inhomogeneous* flows in confined geometries, as may be relevant to transport of cells and vesicles in microcirculation and drug delivery using multiple emulsions.

* Corresponding author. Address: Department of Chemical and Biological Engineering, University of British Columbia, Vancouver, BC, Canada V6T 1Z3.
E-mail address: jfeng@CHML.UBC.CA (J.J. Feng).

0301-9322/$ - see front matter
doi:10.1016/j.ijmultiphaseflow.2007.09.002

Simulating the deformation of a compound drop is a computational challenge because of the two moving and deforming interfaces. Recently, we have developed a diffuse-interface method that accounts for the moving interfaces in a variational framework (Yue et al., 2004; Feng et al., 2005). Implemented using finite elements with adaptive meshing, the method has been applied successfully to several problems in drop dynamics (Yue et al., 2006a; Yue et al., 2006b). In particular, we simulated the deformation of a simple drop through a contraction in a pressure-driven pipe flow (Zhou et al., 2007). This note represents an application of the same methodology to compound drops deformation. The geometry is a prototype for entry of eukaryotic cells into capillaries or micropipettes (Wiggs et al., 1994; Hochmuth, 2000) and the transport of double emulsions (Garti, 1997). It generates a mixed-type flow having shear and extensional characters in different regions, and is thus an extension of prior studies in simple shear and uniform elongational flows.

2. Theory and numerical methods

We treat the interface between two nominally immiscible fluids as a thin but finite mixing layer characterized by a capillary width ϵ and a Ginzburg–Landau mixing energy in terms of a phase field ϕ (Lowengrub and Truskinovsky, 1998). In such a diffuse-interface framework, the scalar field ϕ determines the position of the interface, and the governing equations can be written uniformly throughout the two-phase system. The interfacial tension arises from the mixing energy density, and appears in the momentum equation as a forcing term. A more detailed discussion of the advantages and disadvantages of the diffuse-interface model, vis-à-vis the classical sharp-interface model and other interface regularization methods, can be found in the literature (Lowengrub and Truskinovsky, 1998; Yue et al., 2004; Feng et al., 2005).

Since a compound drop consists of three fluid components separated by two interfaces, a general diffuse-interface representation requires the introduction of an additional phase field and additional interaction energies. The resulting theoretical model is rather complex and cumbersome for numerical computations (Kim et al., 2004). In this initial study, therefore, we have limited ourselves to the W/O/W type of compound drops made of two rather than three fluid components. Then the conventional phase-field description is adequate as the innermost and outermost fluids are identical. This simplified model allows exploration of the fundamental hydrodynamic mechanisms, but precludes a comprehensive parametric study of general three-component compound drops.

The system of equations governing the motion of a two-component Newtonian mixture is as follows (Yue et al., 2004):

$$\nabla \cdot \boldsymbol{v} = 0, \tag{1}$$

$$\rho\left(\frac{\partial \boldsymbol{v}}{\partial t} + \boldsymbol{v}\cdot\nabla\boldsymbol{v}\right) = -\nabla p + \nabla\cdot\{\mu[\nabla\boldsymbol{v} + (\nabla\boldsymbol{v})^{\mathrm{T}}]\} + G\nabla\phi, \tag{2}$$

$$\frac{\partial\phi}{\partial t} + \boldsymbol{v}\cdot\nabla\phi = \gamma\nabla^2 G, \tag{3}$$

$$G = \lambda\left[-\nabla^2\phi + \frac{\phi(\phi^2-1)}{\epsilon^2}\right], \tag{4}$$

where G is the chemical potential and γ is the mobility parameter; λ and ϵ are the interfacial energy density and capillary width, respectively. The phase field ϕ takes on values of ± 1 in the two bulk phases, and the average density and viscosity are simply $\rho = \frac{1+\phi}{2}\rho_1 + \frac{1-\phi}{2}\rho_2$ and $\mu = \frac{1+\phi}{2}\mu_1 + \frac{1-\phi}{2}\mu_2$. Note that the $G\nabla\phi$ term in the momentum equation is a diffuse-interface representation of the interfacial tension. The interface typically has a thickness $\sim 5\epsilon$; the Cahn–Hilliard equation (Eq. 3) ensures that it neither collapses into a sharp surface nor diffuses into a wide region. In the limit of $\epsilon \to 0$, the above system reduces to the familiar sharp-interface formulation, and $2\sqrt{2}\lambda/(3\epsilon)$ gives the interfacial tension σ (Yue et al., 2004).

To accurately capture the interfacial tension, we must use an ϵ that is much smaller than the overall dimension and then resolve the ϕ profile adequately within the thin interface. For this purpose, we have developed a finite-element package AMPHI (Adaptive Meshing with phase field ϕ) that has adaptive meshing as an essential ingredient. Yue et al. (2006b) have described the algorithm in detail and validated the numerical toolkit by

benchmark problems. In the following, we use unstructured triangular elements in an axisymmetric computational domain, with time steps and grid sizes that are fine enough to ensure accuracy of the numerical results.

3. Numerical results

The axisymmetric flow geometry is illustrated in Fig. 1, consisting of two cylindrical tubes connected by a circular arc. The downstream tube has radius a and length $L = 10a$, while the upstream tube is twice as thick with a length of $8a$. The compound drop has a core fluid of density ρ_c and viscosity μ_c, and a shell fluid of ρ_s and μ_s. As mentioned above, the suspending fluid (matrix) is identical to the core fluid. The core–shell and shell–matrix interfaces have the same constant interfacial tension σ. Initially, the two interfaces are concentric and spherical with radii r_c and r_s, centered at $z = 6a$, and there is no flow throughout the domain. At $t = 0$, a constant pressure drop ΔP is applied over the entire length ($19a$) of the domain. On the upstream and downstream boundaries ($z = 0$ and $19a$), we set the boundary conditions to $v_r = 0$ and $\frac{\partial v_z}{\partial z} = 0$. On the centerline we use symmetry conditions: $v_r = 0$ and $\frac{\partial v_z}{\partial r} = 0$. Thus, the flow rate Q varies as the drop traverses the conduit. To construct the dimensionless groups controlling the process, we use a as the characteristic length and $V = \Delta P a^2/(8\mu_c L)$ as the characteristic velocity. Note that V is the average velocity in a Poiseuille flow through a uniform pipe of radius a with pressure gradient $\Delta P/L$. Then six dimensionless groups can be constructed:

$$Ca = \frac{\mu_c V}{\sigma}, \tag{5}$$

$$Re = \frac{\rho_c V a}{\mu_c}, \tag{6}$$

$$\alpha = \frac{\rho_s}{\rho_c}, \tag{7}$$

$$\beta = \frac{\mu_s}{\mu_c}, \tag{8}$$

$$\zeta_c = \frac{r_c}{a}, \tag{9}$$

$$\zeta_s = \frac{r_s}{a}, \tag{10}$$

where the capillary number Ca indicates the ratio between viscous and capillary forces, and the Reynolds number Re represents the ratio between inertial and viscous forces. The characteristic flow time is $t_f = a/V$, and the flow rate will be scaled by $Q_f = \pi a^2 V$. For brevity, we use the same symbols for dimensional and dimensionless variables, but will explicitly indicate which is meant where confusion may arise. In the simulations presented here, we have fixed $\alpha = 1$, $\beta = 1$ and $\zeta_s = 1.4$. We will explore a range of ζ_c to examine the core size effect on the transit process.

The entry of the compound drop into the contraction consists of three distinct stages, which are illustrated by the snapshots of Fig. 2 and the temporal variations of the instantaneous flow rate and drop length in Fig. 3. In the first stage ($0 < t < 4$), the compound drop approaches the contraction. The strong elongational flow causes the shell to form a protrusion, while the core also experiences moderate deformation. The shoulder of the drop progressively blocks the flow area at the contraction, thus causing the continual decrease in flow rate Q (Fig. 3a). The length of the drop l increases in the mean time (Fig. 3b). At the beginning of the second

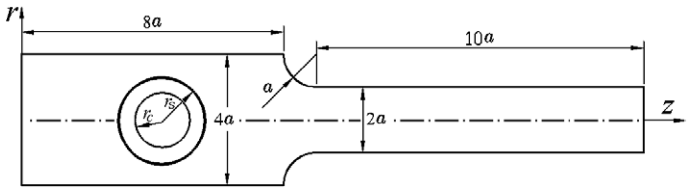

Fig. 1. Geometric setup for simulating the deformation of a compound drop through a 2:1 contraction. Two cylindrical tubes are connected by an arc of radius a and central angle 90°. Shown is the meridian plane and the upper half is the computational domain.

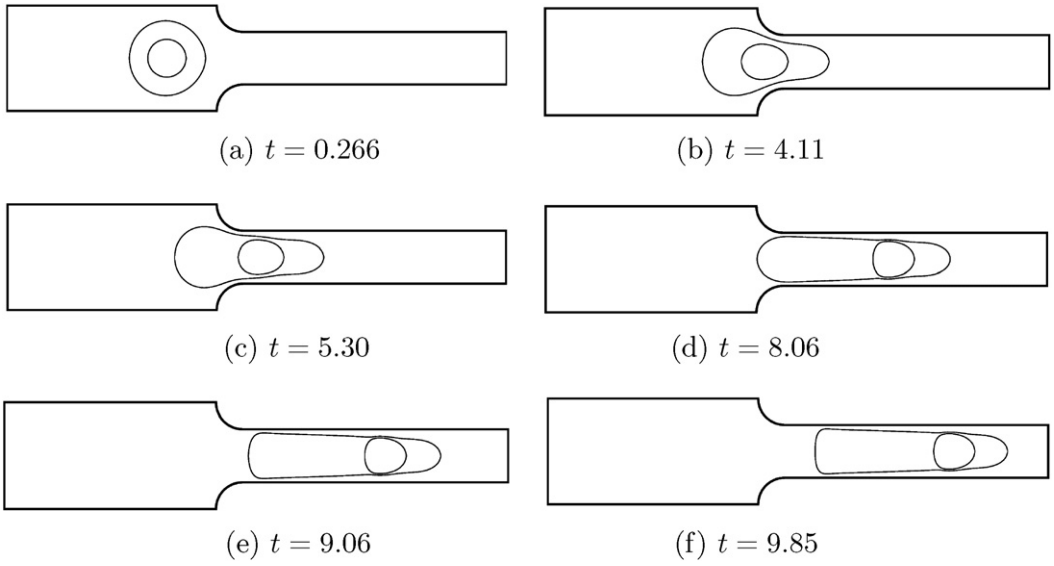

Fig. 2. Snapshots of the transit of a compound drop into the capillary. $Ca = 0.179$, $Re = 1.56 \times 10^{-2}$ and $\zeta_c = 0.72$. Time is scaled by a/V.

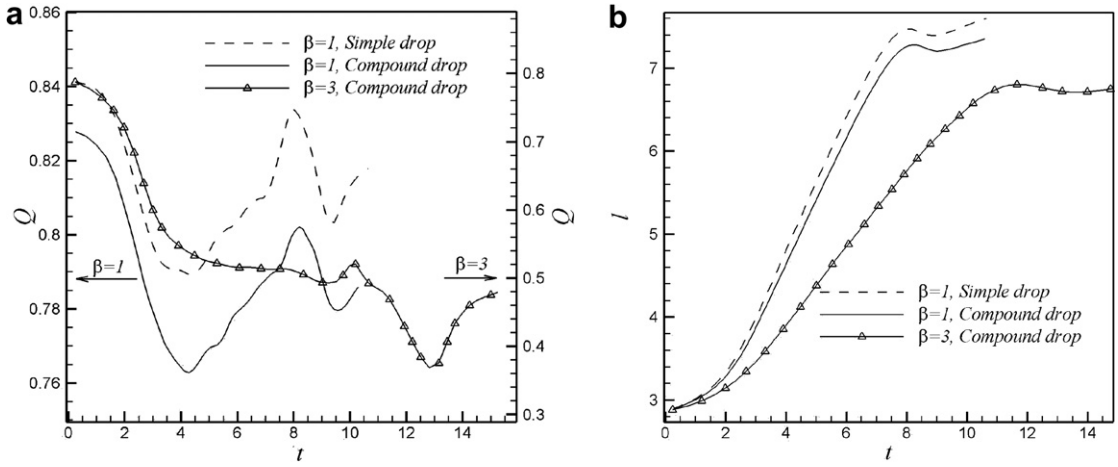

Fig. 3. Temporal variations of the instantaneous flow rate Q and the length of the compound drop l for the process of Fig. 2. For comparison, we have also plotted results for a simple drop of the same size (radius $1.4a$) and fluid properties as well as for a compound drop with a more viscous shell ($\beta = 3$).

stage ($4 < t < 8$), maximum blockage at the contraction corresponds to a minimum Q. Afterwards, the core moves forward along with the shell fluid, thereby deflating the rear of the drop (Fig. 2c). This enlarges the gap between the outer surface and the wall at the contraction and causes a recovery of Q in stage two. Note the small dip in the $Q(t)$ curve at $t = 5$; it is the result of the core passing the constriction. At the end of the second stage, both the flow rate Q and the drop length achieve a local maximum. In stage three ($t > 8$), the rear of the drop, consisting of only the shell fluid, passes the contraction into the thinner tube. As the contraction loses its "grip" on the drop (Fig. 2d), the capillary pressure due to the high curvature in its rear produces a sudden forward flow and a temporary retraction of the drop's overall length (Fig. 3b). This temporary shortening of the drop in turn increases the blockage in the capillary (Fig. 2e) and causes the flow rate to drop sharply (Fig. 3a). Then both Q and l recover as the compound drop translates in the downstream tube. Simulations

using longer tubes indicate that Q and l approach roughly constant values. But the core continues to move slowly forward relative to the shell fluid. This will be seen (cf. Fig. 5) as due to the recirculation in the shell fluid. Eventually the two interfaces are pressed into each other and the shell breaks. Diffuse interfaces are known to coalesce prematurely (Yue et al., 2006a), and the rupture of the shell may not reflect reality.

Qualitatively, the transit process is similar to that of a simple drop, which is also shown in Fig. 3 for comparison. But the core tends to resist deformation of the compound drop and this modifies the process quantitatively. Throughout the drop entry, both Q and l are below those for the simple drop. The fluctuation in Q also has larger magnitudes. After the core is inside the capillary, its surface hampers the recirculation in the shell fluid and causes a slight bulge on the outer surface (Fig. 2c onward). A more viscous core ($\beta < 1$) should amplify these differences although we have not explored this systematically. Note that in terms of suppressing the flow rate and drop deformation, the presence of the core is tantamount to an elevated viscosity in a simple drop (Zhou et al., 2007). From an energetic viewpoint, the impenetrable inner surface causes more dissipation inside the compound drop, and deformation of the inner drop entails an additional energy penalty in the increased interface area.

We have also explored the effect of a more viscous shell fluid as is relevant to typical W/O/W emulsions. The most prominent difference from the equal-viscosity case occurs in the second stage (Fig. 3). Instead of a strong recovery, Q remains more or less constant, or even decrease somewhat for larger β. This is because a more viscous shell reacts more slowly to the ambient flow. As the core enters the downstream tube, the rear of the drop does not deflate rapidly enough to boost the total flow rate Q. By the same token, the cell length l is generally smaller for larger β, and the transit time τ_{trans} is longer. The effect of shell viscosity is similar to that of the drop viscosity for a simple drop (Zhou et al., 2007).

It is no surprise that the compound drop takes longer time to traverse the passage than a simple drop of the same size. Fig. 4(a) plots the "transit time" τ_{trans}, defined as the interval between the moments when the leading and trailing edges of the drop enter the thinner tube, as a function of the capillary number. As τ_{trans} has been scaled by the flow time $t_f = a/V$, its increase with Ca does not withstand the decrease of the *dimensional* transit time with the pressure drop or flow rate. Surprisingly, τ_{trans} shows a non-monotonic dependence on the core size ζ_c (Fig. 4b). Intuitively one expects τ_{trans} to increase with ζ_c since the larger the inner drop, the larger the energy penalty in deforming it so that the drop can enter the capillary. This seems to hold for ζ_c up to 0.6. To understand the anomalous decrease of τ_{trans} for larger ζ_c, we compare the flow patterns for $\zeta_c = 0.64$ and 0.80 in Fig. 5.

When the drop first approaches the entry, the above intuition is indeed borne out and the drop with the larger core attains a lower speed. After the core completely enters the capillary, however, the larger core,

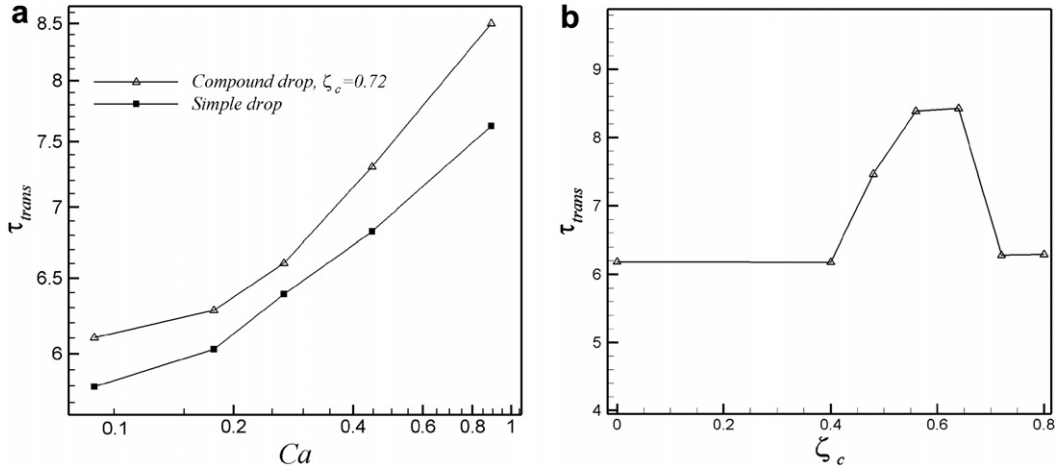

Fig. 4. (a) Effect of the inner drop on the transit time with changing pressure drop with $\zeta_c = 0.72$. The Reynolds number varies in the range $7.81 \times 10^{-3} \leqslant Re \leqslant 7.81 \times 10^{-2}$. (b) Transit time as a function of the core radius, represented by ζ_c, at $Ca = 0.179$ and $Re = 1.56 \times 10^{-2}$. In both plots the size of the outer drop is fixed with $\zeta_s = 1.4$.

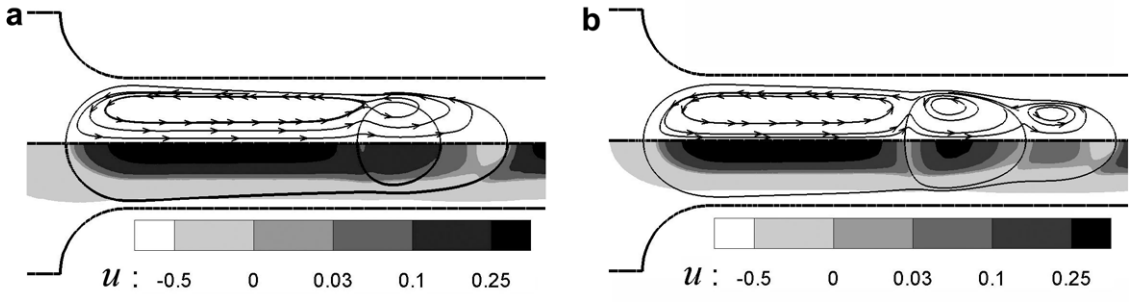

Fig. 5. Flow fields inside the compound drop toward the end of the entry process for two core radii: (a) $\zeta_c = 0.64$, (b) $\zeta_c = 0.80$. In both cases, $Ca = 0.179$, $Re = 1.56 \times 10^{-2}$. The streamlines are drawn in a reference frame fixed to the leading edge of the compound drop, which has an instant velocity of $0.81V$ in (a) and $1.21V$ in (b). The gray-scale contours are for the horizontal velocity u.

though more elongated, requires no additional energy to maintain its shape. Now the smaller inner drop continues to move forward relative to the outer drop surface (Fig. 5a); its instantaneous velocity is $0.11V$ relative to the front tip of the compound drop. But the larger core has practically stopped moving forward as a whole (Fig. 5b), with a relative velocity of $0.012V$. Meanwhile, internal eddies develop within the inner drop in Fig. 5b to accommodate the recirculation in the shell fluid. As a consequence, the smaller core in Fig. 5a creates *stronger velocity gradients* on its flanks than the larger core. This translates to a larger drag on the compound drop in Fig. 5a and a lower speed. This explains the shorter transit time for the drop with the larger core.

The difference in drop speed is reflected by the flow rate. The instantaneous Q at the moment when the drop completely enters the smaller tube is also a non-monotonic function of ζ_c. Besides, one notes the greater drop length l in Fig. 5b with the larger core. This contrasts the trend in Fig. 3b and confirms that the drop length also varies non-monotonically with the core size. With even larger ξ_c, however, the trend is bound to reverse once more since in the limit of $\xi_c \to \xi_s$, the compound drop approaches a simple one with twice the interfacial tension.

It is interesting to compare our results with compound drop deformation in *unbounded elongational flows*. With $\beta = 1$, equal interfacial tension on the inner and outer surfaces and $r_c = 0.5r_s$, Stone and Leal (1990) and Kan et al. (1998) found that for capillary numbers much below the critical value Ca_{cr} for breakup, the deformation of the compound drop in an elongational flow is nearly the same as a simple drop of the same fluid and size. This is because the recirculation within the shell fluid is weak and the core deforms little. Thus, the inner surface hardly hinders the overall deformation of the drop. As Ca approaches Ca_{cr}, however, the shell is so stretched that the outer interface presses against the core. Then the core does affect the deformation and breakup of the compound drop (Stone and Leal, 1990; Kan et al., 1998). In our confined flow geometry, on the other hand, the compound drop is subject to a geometric constraint that dictates the deformation of the inner drop as well as the shell, regardless of the capillary number. Hence the compound drop sustains milder deformation than the simple drop in Fig. 3, and the difference increases with flow speed or Ca. Obviously, as ζ_c becomes sufficiently small, the difference between simple and compound drop deformation should vanish.

4. Summary

This note presents simulations of the morphological evolution of a compound drop as it moves along the centerline of a circular tube with a 2:1 gradual contraction. The flow is driven by a fixed pressure difference imposed on the matrix fluid. The deformation of the two interfaces is captured by a phase-field representation, with an interfacial tension determined by the mixing energy in the thin but diffuse interfaces. Results show that the inner core generally hinders deformation of the compound drop and prolongs the transit time. However, the effect is non-monotonic in the core size; it is greatest for an intermediate core radius. The underlying mechanism is the core hampering the inner circulation and subjecting the compound drop to stronger shear inside the shell.

The expedient of using a *binary* phase-field model places a limitation on our study: the inner core fluid must be identical to the suspending fluid. This is appropriate for W/O/W compound drops encountered in drug delivery. A more general compound drop involves three different fluid components. Such systems call for tertiary phase-field models as have recently appeared in the literature (Kim et al., 2004; Burman et al., 2004). For example, a white blood cell has a nucleus that is much more viscous than the cytoplasm, which is in turn different from the suspending plasma. Biological cells, of course, contain additional complexities such as membrane elasticity that are not easily represented in a compound drop model.

Acknowledgments

Acknowledgment is made to the Donors of The Petroleum Research Fund, administered by the American Chemical Society, for partial support of this research. J.J.F. was also supported by the NSERC, the Canada Research Chair program and the Canada Foundation for Innovation. C.Z. acknowledges partial support by a University Graduate Fellowship from UBC.

References

Bozkir, A., Hayta, G., 2004. Preparation and evaluation of multiple emulsions water-in-oil-in-water (w/o/w) as delivery system for influenza virus antigens. J. Drug Target. 12, 157–164.

Burman, E., Jacot, A., Picasso, M., 2004. Adaptive finite elements with high aspect ratio for the computation of coalescence using a phase-field model. J. Comput. Phys. 195, 153–174.

Engel, R.H., Riggi, S.J., Fahrenbach, M.J., 1968. Insulin: intestinal absorption as water-in-oil-in-water emulsions. Nature 219, 856–857.

Feng, J.J., Liu, C., Shen, J., Yue, P., 2005. An energetic variational formulation with phase field methods for interfacial dynamics of complex fluids: advantages and challenges. In: Calderer, M.-C.T., Terentjev, E.M. (Eds.), Modeling of Soft Matter. Springer, NewYork, pp. 1–26.

Garti, N., 1997. Double emulsions – scope, limitations and new achievements. Colloid Surf. A 123–124, 233–246.

Goubault, C., Pays, K., Olea, D., Gorria, P., Bibette, J., Schmitt, V., Leal-Calderon, F., 2001. Shear rupturing of complex fluids: Application to the preparation of quasi-monodisperse water-in-oil-in-water double emulsions. Langmuir 17, 5184–5188.

Hochmuth, R.M., 2000. Micropipette aspiration of living cells. J. Biomech. 33, 15–22.

Jadhav, S., Eggleton, C.D., Konstantopoulos, K., 2005. A 3-D computational model predicts that cell deformation affects selectin-mediated leukocyte rolling. Biophys. J. 88, 96–104.

Jiao, J., Burgess, D.J., 2003. Rheology and stability of water-in-oil-in-water multiple emulsions containing Span 83 and Tween 80. AAPS PharmSci. 5, Article 7.

Johnson, R.E., Sadhal, S.S., 1985. Fluid mechanics of compound multiphase drops and bubbles. Annu. Rev. Fluid Mech. 17, 289–320.

Kan, H.C., Udaykumar, H.S., Shyy, W., Tran-Son-Tay, R., 1998. Hydrodynamics of a compound drop with application to leukocyte modeling. Phys. Fluids 10, 760–774.

Khismatullin, D.B., Truskey, G.A., 2005. Three-dimensional numerical simulation of receptor-mediated leukocyte adhesion to surfaces: Effects of cell deformability and viscoelasticity. Phys. Fluids 17, 031505–031521.

Kim, J., Kang, K., Lowengrub, J., 2004. Conservative multigrid methods for ternary Cahn-Hilliard systems. Commun. Math. Sci. 2, 53–77.

Lowengrub, J., Truskinovsky, L., 1998. Quasi-incompressible Cahn–Hilliard fluids and topological transitions. Proceedings of the Royal Society of London. Series A 454, 2617–2654.

Muguet, V., Seiller, M., Barratt, G., Ozer, O., Marty, J.P., Grossiord, J.L., 2001. Formulation of shear rate sensitive multiple emulsions. J. Controll. Release 70, 37–49.

Onuki, Y., Morishita, M., Takayama, K., 2004. Formulation optimization of water-in-oil–water multiple emulsion for intestinal insulin delivery. J. Controll. Release 97, 91–99.

Smith, K.A., Ottino, J.M., de la Cruz, M.O., 2004. Encapsulated drop breakup in shear flow. Phys. Rev. Lett. 93, 204501.

Stone, H.A., Leal, L.G., 1990. Breakup of concentric double emulsion droplets in linear flows. J. Fluid Mech. 211, 123–156.

Stroeve, P., Varanasi, P.P., 1984. An experimental-study on double emulsion drop breakup in uniform shear-flow. J. Colloid Interf. Sci. 99, 360–373.

Toose, E.M., Geurts, B.J., Kuerten, J.G.M., 1999. A 2D boundary element method for simulating the deformation of axisymmetric compound non-Newtonian drops. Int. J. Numer. Methods Fluids 30, 653–674.

Utada, A.S., Lorenceau, E., Link, D.R., Kaplan, P.D., Stone, H.A., Weitz, D.A., 2005. Monodisperse double emulsions generated from a microcapillary device. Science 308, 537–541.

Wiggs, B.R., English, D., Quinlan, W.M., Doyle, N.A., Hogg, J.C., Doerschuk, C.M., 1994. Contributions of capillary pathway size and neutrophil deformability to neutrophil transit through rabbit lungs. J. Appl. Phys. 77, 463–470.

Yue, P., Feng, J.J., Liu, C., Shen, J., 2004. A diffuse-interface method for simulating two-phase flows of complex fluids. J. Fluid Mech. 515, 293–317.

Yue, P., Zhou, C., Feng, J.J., 2006a. A computational study of the coalescence between a drop and an interface in Newtonian and viscoelastic fluids. Phys. Fluids 18, 102102.

Yue, P., Zhou, C., Feng, J.J., Ollivier-Gooch, C.F., Hu, H.H., 2006b. Phase-field simulations of interfacial dynamics in viscoelastic fluids using finite elements with adaptive meshing. J. Comput. Phys. 219, 47–67.

Zhou, C., Yue, P., Feng, J.J., 2006. Formation of simple and compound drops in microfluidic devices. Phys. Fluids 18, 092105.

Zhou, C., Yue, P., Feng, J.J., 2007. Simulation of neutrophil deformation and transport in capillaries using simple and compound drop models. Ann. Biomed. Eng. 35, 766–780.